

π^-p Reactions at 456, 505, and 552 MeV/c†

D. H. SAXON AND J. H. MULVEY

Nuclear Physics Department, Keble Road, Oxford, England

AND

W. CHINOWSKY

Lawrence Radiation Laboratory, Berkeley, California 94720

(Received 1 May 1970)

We present the results of an experiment to study the reactions $\pi^-p \rightarrow \pi\pi N$ at incident momenta of 456, 505, and 552 MeV/c in a hydrogen bubble chamber. The most prominent features of the data in the $\pi^+\pi^-n$ final state are a high-mass peak in the $M^2(\pi^+\pi^-)$ spectrum (which moves upward in mass and becomes less significant as the incident momentum increases), and Δ^- production. We show that the $\pi^+\pi^-$ enhancement can be explained by the introduction of an $I=J=0$ $\pi\pi$ interaction, and investigate two forms for this interaction. Within the framework of an isobar model, we derive values of the πN partial-wave inelasticities and compare these with the predictions of πN elastic phase-shift analyses. It is shown that the branching ratio $\pi N:\pi\Delta:\sigma N$ of the P_{11} partial wave depends strongly on the assumed form of $\pi\pi$ final-state interaction.

I. INTRODUCTION

THIS paper describes the analysis of new data on the reactions $\pi^-p \rightarrow \pi^-p$ and $\pi^-p \rightarrow \pi\pi N$ (chiefly $\pi^+\pi^-n$) at incident momenta of 456, 505, and 552 MeV/c.

In previous studies of these reactions at similar energies,^{1,2} a broad enhancement was observed, at about 400 MeV/c², in the $\pi^+\pi^-$ mass spectrum which was absent in the $\pi^-\pi^0$ distribution. It has been a principal purpose of this experiment to obtain sufficient statistical accuracy to enable a detailed analysis of these final states to be made and to find an explanation of this effect. At the same time the analysis provides information, which was previously lacking, on the partial-wave inelasticities and branching ratios of the πN system in the mass range 1338–1402 MeV/c². (Work in progress will extend the range to 1300–1520 MeV/c².) At these energies the only inelastic channels are to three-body final states, with consequent uncertainties in interpretation, owing to the need for a model if useful information is to be obtained. Pion-nucleon s -channel processes are expected to dominate at these low energies; there is no evidence of the presence of exchange mechanisms, and so they have not been considered in the analysis. The so-called “isobar model”³ is used here.

† Work supported in part by the United Kingdom Science Research Council and in part by U. S. Atomic Energy Commission.

¹ J. Kirz, J. Schwartz, and R. D. Tripp, *Phys. Rev.* **130**, 2481 (1963).

² C. N. Vittitoe, B. R. Riley, W. J. Fickinger, V. P. Kenney, J. G. Mowat, and W. D. Shephard, *Phys. Rev.* **135**, B232 (1964); S. Femino, S. Janelli, and F. Mezzanares, *Nuovo Cimento* **52A**, 892 (1967); L. Bertanza, A. Bigi, R. Carrara, and R. Casali, *ibid.* **44A**, 712 (1966); R. A. Burnstein, G. R. Charlton, T. B. Day, G. Quareni, A. Quareni-Vignudelli, G. B. Yodh, and I. Nadelhaft, *Phys. Rev.* **138**, B1044 (1965); J. D. Oliver, I. Nadelhaft, and G. B. Yodh, *ibid.* **147**, 932 (1966); M. Banner, J. F. Deteouf, M. L. Fayoux, J. L. Hamel, J. Zsembery, J. Cheze, and J. Teiger, *ibid.* **166**, 1346 (1968).

³ R. Sternheimer and S. Lindenbaum, *Phys. Rev.* **109**, 1723 (1958).

In the model, coherent production of $\pi\Delta$ and $N\sigma$ is assumed, where σ is an $I=J=0$ state of two pions. The formulation of this model and its inherent difficulties are discussed in Sec. IV. The data are described in Sec. II; the elastic differential cross-section and inelastic cross-section determination are dealt with in Sec. II B. Section III gives the results of a model-independent moments analysis. The isobar model is fitted to the data in Sec. V. In Sec. VI predictions are made of πN partial-wave inelasticities and compared with those of elastic phase-shift analyses⁴ and in Sec. VII the P_{11} branching ratio is calculated. Section VIII summarizes the conclusions of this work.

II. EXPERIMENTAL DETAILS AND DATA

A. Experiment

The Saclay 180-liter (80-cm) hydrogen bubble chamber was exposed to incident negative pions at the NIMROD accelerator of the Rutherford High Energy Laboratory. In the exposure 145 000 pictures were taken at 456 MeV/c, 85 000 at 505 MeV/c, and 45 000 at 552 MeV/c.

Especially at the lowest momentum, contamination of the beam with electrons and muons was a serious problem and to eliminate electrons in the run at 456 MeV/c, a $\frac{1}{8}$ -in. Pb foil was put in the beam at an intermediate focus. A bending magnet removed degraded electrons from the beam before it entered the bubble chamber.

Scanning and measuring of the lower-momenta film were done at Oxford University Nuclear Physics Laboratory; the 552-MeV/c exposure was processed at the Lawrence Radiation Laboratory. Measurements at both laboratories were made with image plane digitizers having setting accuracy about 7μ on film.

⁴ R. Plano, in *Proceedings of the Lund International Conference on Elementary Particles, 1969*, edited by G. von Dardel (Berlingska, Lund, Sweden, 1969).

The reactions giving rise to two-prong events are

$$\pi^- + p \rightarrow \pi^- + p \quad (1)$$

$$\rightarrow \pi^- + p + \pi^0 \quad (2)$$

$$\rightarrow \pi^- + \pi^+ + n. \quad (3)$$

Of these the elastic scattering (1) is most common and reaction (2) is the rarest, having only about one-fifth the number of events of reaction (3). The cross section for four-prong events is very small (less than ten events seen), and contamination of reaction (2) by cases of $\pi^-p\pi^0\pi^0$ is entirely negligible.

The film with the lower-momenta incident pions was prescanned to select examples of the reaction $\pi^-p \rightarrow \pi^-\pi^+n$ among the much more numerous elastic scatterings; criteria based on bubble density and curvature of the positive tracks readily permitted elimination of events with proton rather than π^+ tracks. In case of doubt the event was measured. In all such situations, kinematic identification of the tracks provided an unambiguous selection. Since it is not possible to select examples of $\pi^-p \rightarrow \pi^-\pi^0p$ using only visual criteria and it was not feasible to measure all events ($\sim 20\,000$ at 505 MeV/c, $\sim 35\,000$ at 456 MeV/c), the data at these two momenta are restricted to the $\pi^-\pi^+n$ channel and, in the 505-MeV/c data, a sample of other events randomly selected from a subset of events obtained with the $\frac{1}{8}$ -in. Pb foil in the beam. The mean incident momentum for these events was 499 MeV/c. This group includes elastic scatters and a small number of π^0 production events.

All events were measured in the film with 552-MeV/c incident pions. Those data contain events in both inelastic channels, as well as elastic scatters. Part of the film was scanned twice to provide a measure of the scanning efficiency for different classes of events. After eliminating events not satisfying incident track momentum and entrance-angle criteria, those outside the chosen fiducial volume and with confidence level $< 1\%$, there resulted the numbers of events, in the various final states, listed in Table I. The 528 examples of $\pi^-\pi^0p$, at the highest momentum, were selected using the standard techniques of selection based on consistency of the measured quantities with the appropriate

TABLE I. Numbers of events.

Momentum (MeV/c)		No. of events after cuts		
Central value	Limits accepted	π^-p	$\pi^+\pi^-n$	$\pi^-p\pi^0$
456 ^a	440-470		2591	
499 ^b	482-516	1386	298	47
505	490-520		1965	
552	536-566	6503	2241	528

^a Film taken with a $\frac{1}{8}$ -in. lead sheet at a double focus of the beam to reduce electron contamination.

^b Film taken with $\frac{1}{8}$ -in. lead sheet in the beam. The 298 $\pi^+\pi^-n$ events are included within the 1965 $\pi^+\pi^-n$ events having 505 MeV/c average momentum.

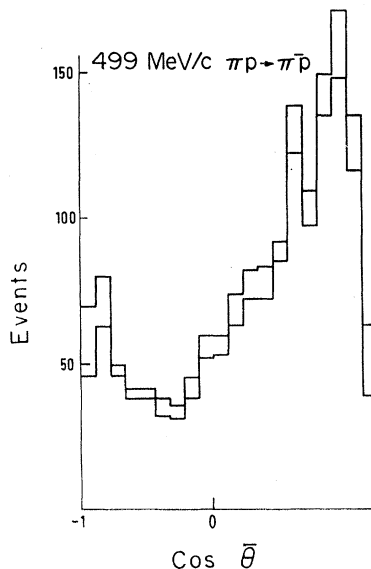


FIG. 1. Elastic c.m. scattering angular distribution at 499 MeV/c incident π^- momentum. The upper histogram gives the data after corrections for scanning losses; the lower shows raw data.

kinematical constraints. In cases where the identification was ambiguous between an inelastic mode and an elastic, the event was assigned to the elastic category. These were small enough in number so that there is no significant contamination, or loss, of events in the $\pi^-\pi^0p$ data.⁵ No physically significant biases were discovered, in a thorough search, except in the elastic scattering data, in which extreme forward and backward scatters are sometimes difficult to see. The elastic scattering data in Sec. II B are given after correction for scanning losses. The correction is reliable except for $\cos\theta > 0.9$ (θ is the scattering angle in the c.m. system). A fuller account of the experimental details is given elsewhere.⁶

B. Elastic Scattering and Cross-Section Normalization

In Figs. 1 and 2 the distributions in $\cos\theta$ for elastic scatters at the two higher momenta are shown.^{7,8} Both the raw data (lower histogram) and that corrected for scanning losses (upper histogram) are presented.

To obtain total cross sections for inelastic reactions, we normalize to the elastic scattering differential cross

⁵ $\pi^-p/\pi^-p\pi^0$ ambiguities arise chiefly in backwards elastic scatters, the number of which is not large. The effect of the scanning loss of short-proton events on the $\pi^-\pi^0$ mass spectrum has been calculated and shown to be spread over a range of masses and always less than the statistical error. [The loss is typically $(3\pm 1)\%$ in the mass range 280-300 MeV/c².]

⁶ D. H. Saxon, Rutherford High Energy Laboratory Report No. HGP/T/6, 1970 (unpublished).

⁷ Within the errors they are consistent with interpolations of the CERN "theoretical" phase shifts; see Ref. 8.

⁸ A. Donnachie, R. G. Kirsopp, and C. Lovelace, CERN Report No. CERN/TH 838, addendum (unpublished).

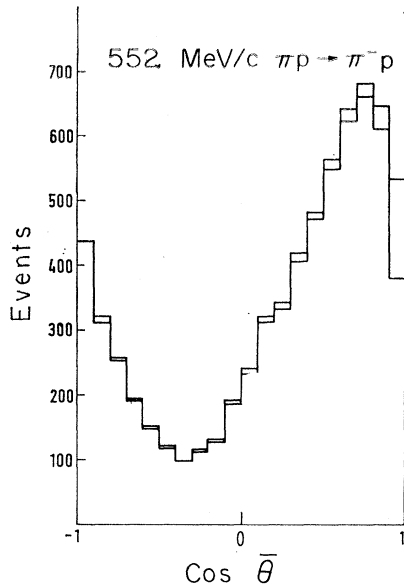


FIG. 2. Elastic c.m. scattering angle distribution at 552 MeV/c incident π^- momentum. The upper histogram gives the data after corrections for scanning losses; the lower shows raw data.

sections of Ogden *et al.*⁹ This procedure is more reliable than incident beam track counting, first because of the unknown contamination of electrons and muons in the beam and second the relative scanning efficiencies can be evaluated better than the absolute.

The cross section in the range $-0.9 < \cos\bar{\theta} < 0.5$, which is least affected by scanning losses and varies slowly with incident momentum, was interpolated between the Ogden *et al.* data. The results are given in Table II. For information, we include the 456-MeV/c inelastic cross sections from the compilation of Olsson and Yodh.¹⁰ Our values at the higher momenta are in excellent agreement with the data of this compilation.

C. Three-Body Final States

A two-to-three-body reaction is described in its c.m. system by five kinematic variables (ignoring spin). We choose a right-handed axis system in the final state, with the x axis along the outgoing nucleon, and the z axis along $\mathbf{p}_N \times \mathbf{p}_{\pi_1}$, where \mathbf{p}_N and \mathbf{p}_{π_1} are the outgoing

TABLE II. Total cross sections (mb).

Momentum (MeV/c)	$\pi^+\pi^-n$	$\pi^-\pi^0p$
456	1.0 ± 0.2	0.17 ± 0.05
499	2.40 ± 0.16	0.32 ± 0.05
552	3.84 ± 0.16	0.87 ± 0.05

⁹ P. M. Ogden, D. E. Hagge, J. E. Helland, M. Banner, J-F Deteouf, and J. Teiger, Phys. Rev. **137**, B1115 (1965).

¹⁰ M. G. Olsson and G. B. Yodh, Phys. Rev. **145**, 1309 (1966).

momenta of the nucleon and π^+ , in $\pi^+\pi^-n$, or π^- , in $\pi^-\pi^0p$.

Five independent variables are: $s^{1/2}$, the c.m. energy; m_{12} , the invariant mass of particles 1 and 2; m_{23} , the invariant mass of particles 2 and 3; $\cos\Theta$, where Θ is the polar angle of the incident π^- with respect to the axes described above; Φ , the azimuthal angle of the incident π^- . The angles have been used by previous authors.¹¹⁻¹⁶

Other variables may also be defined, viz., m_{13} , the invariant mass of particles 1 and 3, with

$$m_{12}^2 + m_{23}^2 + m_{13}^2 = s + m_1^2 + m_2^2 + m_3^2$$

and $\cos\bar{\theta}_1$, $\cos\bar{\theta}_2$, and $\cos\bar{\theta}_3$ the cosines of the production angles of the three final-state particles. By production angle we mean the angle, in the c.m. system, between the directions of the incident π^- and the outgoing particle.

Figures 3-5 show the Dalitz plots for the $\pi^-\pi^+n$ state at each of the three energies. At all energies a strong concentration is seen at large $\pi^-\pi^+$ effective mass and large π^-n effective mass. Projections on the Dalitz-plot axes, the $\pi^+\pi^-$ and π^-n (mass)² distributions, and, for completeness, the π^+n (mass)² distributions are shown in Figs. 7 and 8 for the 552-MeV/c data, while Figs. 11 and 12 show these mass distributions for the 505- and 456-MeV/c data, respectively. The peaking at high $\pi^-\pi^+$ mass is evident at all three energies. The π^-n distribu-

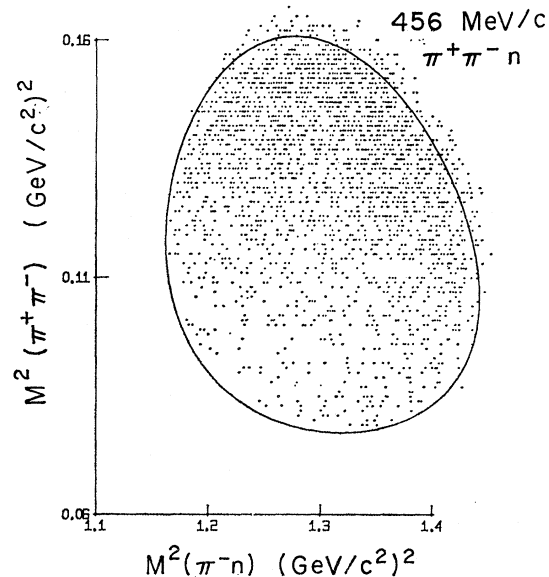


FIG. 3. Dalitz plot for $\pi^-p \rightarrow \pi^+\pi^-n$ at 456 MeV/c.

¹¹ S. M. Berman and M. Jacob, Phys. Rev. **139**, B1023 (1965).

¹² D. Branson, P. V. Landshoff, and J. C. Taylor, Phys. Rev. **132**, 902 (1963).

¹³ R. C. Arnold and J. L. Uretsky, Phys. Rev. **153**, 1443 (1967).

¹⁴ D. Morgan, Phys. Rev. **166**, 1731 (1968).

¹⁵ B. Deler and G. Valladas, Nuovo Cimento **45A**, 559 (1966).

¹⁶ M. G. Bowler and R. J. Cashmore, Nucl. Phys. **B17**, 331 (1970).

tion shifts toward high masses at the higher momenta. These features of the mass spectra were already prominent in the early results of Kirz, Schwartz, and Tripp¹ and led to speculation about a possible $I=0, J=0$ pion-pion resonant final-state interaction. A difficulty with this simple interpretation is that no clearly defined peak above a continuous background appears in the mass distributions. Indeed the maximum in the $\pi^-\pi^+$ mass spectrum moves with incident energy so that it is not possible to define a mass for the conjectured resonance. A more sophisticated formalism, including effects of both $\pi\pi$ and πN final-state interactions, is required for a satisfactory interpretation of the data.

Figures 6-8 show the 552-MeV/c $\pi^-\pi^0p$ Dalitz plot and effective-mass distributions. Compared to the $\pi^-\pi^+n$ data, there appears considerably less evidence for final-state interactions. Neither the $\pi\pi$ or πN mass distributions show strong peaking. This indicates that any strong $\pi\pi$ interaction must be in the isotopic spin-0 state. Differences among the pion-nucleon mass spectra in the two final states can be simply understood as a feature of the production of the $\Delta(1236)$ resonance. Isotopic spin conservation selection rules strongly favor production of the negatively charged isobar and so strongest peaking in the π^-n mass spectrum, as observed.

The distributions in the angles Θ and Φ , the angles of the incident pion direction with respect to the "body-fixed" axes defined above, and the production angles, are shown in Figs. 9-12. Both the $\pi^-\pi^+n$ and $\pi^-\pi^0p$ data are presented. No strong departures from isotropy in the $\cos\Theta$ distributions are noted. However, the azimuthal angular distributions are strongly non-

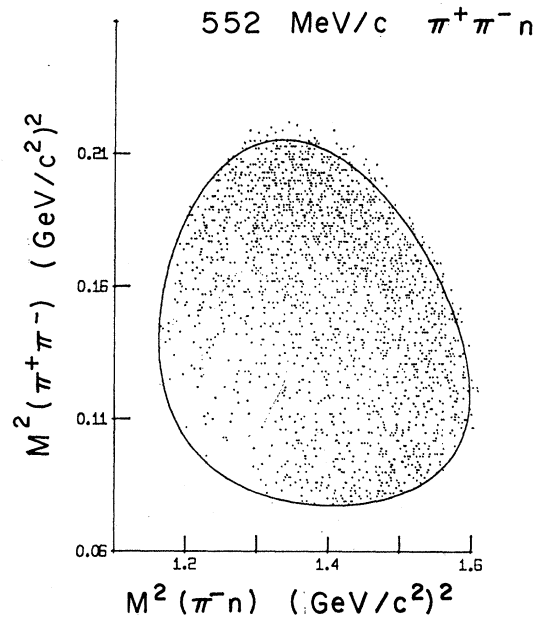


FIG. 5. Dalitz for $\pi^-p \rightarrow \pi^+\pi^-n$ at 552 MeV/c.

isotropic and unsymmetric, even at the lowest energy of the $\pi^-\pi^+n$ state. This anisotropy is also present in the Φ distribution for the $\pi^-\pi^0p$ data but is perhaps not as clearly established because of the severe statistical uncertainties. An immediate conclusion is that at least two angular momentum states of opposite parity contribute to the pion production.

The production angle distributions show no strong forward or backward peaking. This suggests that an

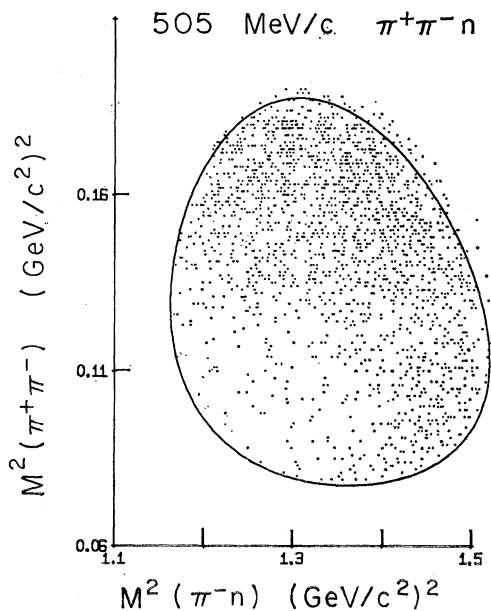


FIG. 4. Dalitz plot for $\pi^-p \rightarrow \pi^+\pi^-n$ at 505 MeV/c.

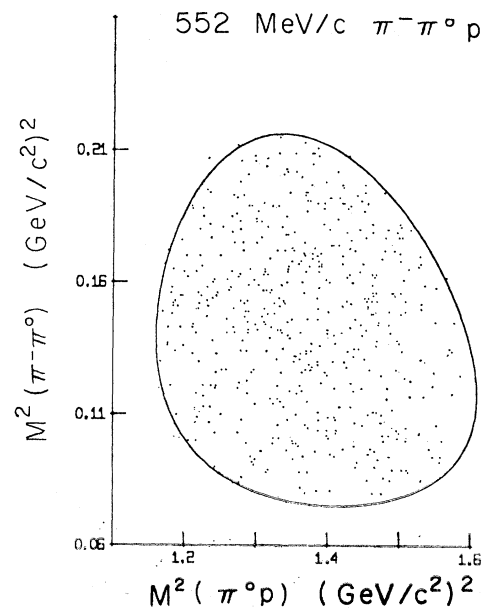


FIG. 6. Dalitz plot for $\pi^-p \rightarrow \pi^-\pi^0p$ at 552 MeV/c.

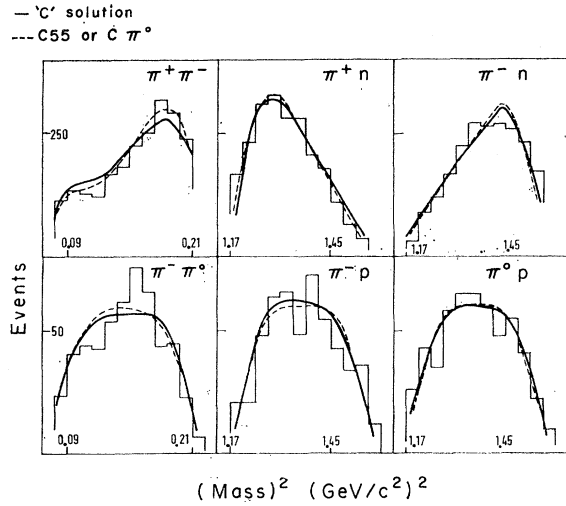


FIG. 7. $(\text{Mass})^2$ spectra at 552 MeV/c. Fitted distributions obtained with the "cube" form of $\pi\pi$ phase shift are superimposed on the experimental histograms.

s -channel model will be particularly simple and involve only a few partial waves. There is no reason to consider t -channel models.

III. MODEL-INDEPENDENT ANALYSIS

Some indication of the magnitude of the various initial-state angular momentum waves present may be inferred, independently of any dynamical assumptions, from the coefficients in an expansion of the production intensity in a series of spherical harmonics. With the variables Θ , Φ , $m_{\pi\pi}$, and $m_{\pi N}$ used here, this is

$$W(\Theta, \Phi, m_{\pi\pi}, m_{\pi N})$$

$$= \sum_{K,M} \left(\frac{2K+1}{4\pi} \right)^{1/2} W_{K^M}(m_{\pi\pi}, m_{\pi N}) Y_{KM}^*(\Theta, \Phi).$$

The expansion coefficients W_{K^M} are functions of position in the Dalitz plot. In principle, a good representation of the experimental results is provided by the dependence of these coefficients upon position in the Dalitz plot. Also, differences in partial-wave contributions to σ production and Δ production may be noted by the variation of these parameters from, for instance, large $\pi\pi$ mass to large πN mass. Unfortunately, the statistical uncertainties in restricted groupings of the data are too severe to permit conclusions, and so we only give the coefficients for the complete samples of data.

Table III gives the values of the W_{K^M} and their errors for $K \leq 5$. All higher moments are, within the errors, consistent with zero. Those moments not given

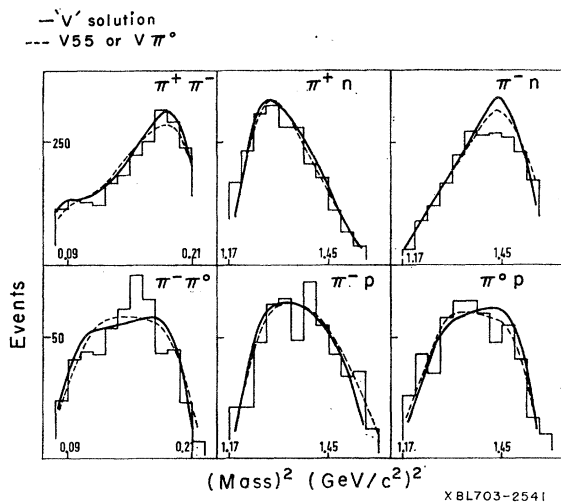


FIG. 8. $(\text{Mass})^2$ spectra at 552 MeV/c. Fitted distributions obtained with the "Veneziano" form of $\pi\pi$ phase shifts are superimposed on the experimental histograms.

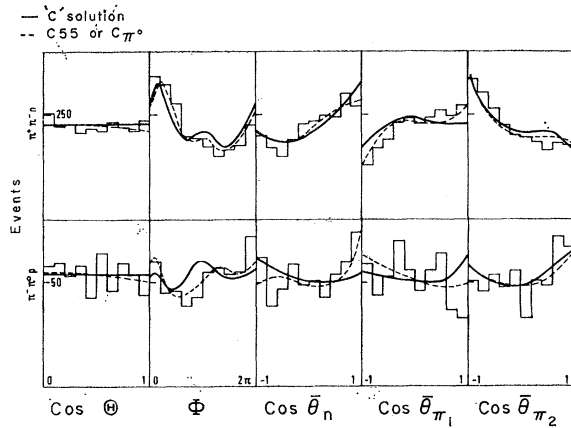


FIG. 9. Angular distributions at 552 MeV/c with "cube" fits.

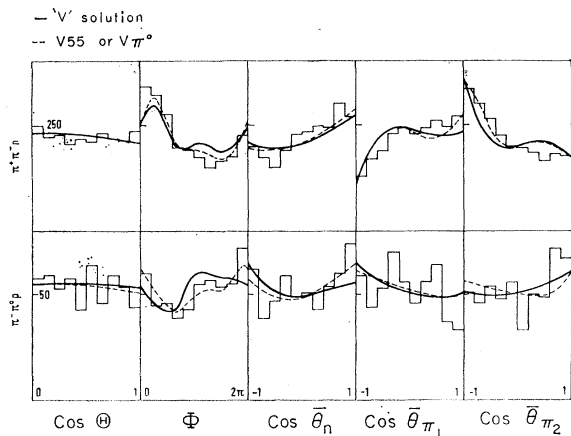


FIG. 10. Angular distributions at 552 MeV/c with "Veneziano" fits.

TABLE III. W_{KM} moments, integrated over the Dalitz plot.

K	M	456 MeV/c $\pi^+\pi^-n$	505 MeV/c $\pi^+\pi^-n$
1	1	$-0.066 \pm 0.008 + i(-0.066 \pm 0.008)$	$-0.055 \pm 0.009 + i(-0.079 \pm 0.009)$
2	0	0.020 ± 0.012	0.023 ± 0.010
2	2	$0.0062 \pm 0.0061 + i(0.018 \pm 0.006)$	$-0.006 \pm 0.006 + i(-0.008 \pm 0.006)$
3	1	$-0.009 \pm 0.005 + i(-0.003 \pm 0.005)$	$0.001 \pm 0.006 + i(-0.013 \pm 0.006)$
3	3	$0.010 \pm 0.005 + i(-0.001 \pm 0.005)$	$0.004 \pm 0.006 + i(-0.008 \pm 0.006)$
4	0	-0.014 ± 0.007	-0.019 ± 0.008
4	2	$-0.007 \pm 0.005 + i(-0.005 \pm 0.005)$	$-0.002 \pm 0.005 + i(0.004 \pm 0.005)$
4	4	$-0.002 \pm 0.005 + i(0.010 \pm 0.005)$	$-0.004 \pm 0.005 + i(0.004 \pm 0.005)$
5	1	$0.003 \pm 0.004 + i(-0.003 \pm 0.004)$	$0.008 \pm 0.005 + i(0.007 \pm 0.005)$
5	3	$0.005 \pm 0.004 + i(0.003 \pm 0.004)$	$0.001 \pm 0.005 + i(0.001 \pm 0.005)$
5	5	$0.002 \pm 0.004 + i(-0.003 \pm 0.004)$	$-0.009 \pm 0.005 + i(-0.003 \pm 0.005)$
		552 MeV/c $\pi^+\pi^-n$	552 MeV/c $\pi^-\pi^0p$
1	1	$-0.070 \pm 0.009 + i(-0.080 \pm 0.008)$	$-0.035 \pm 0.019 + i(0.038 \pm 0.017)$
2	0	-0.001 ± 0.009	-0.019 ± 0.019
2	2	$0.012 \pm 0.007 + i(0.031 \pm 0.007)$	$0.037 \pm 0.014 + i(0.015 \pm 0.014)$
3	1	$-0.014 \pm 0.006 + i(-0.003 \pm 0.006)$	$0.004 \pm 0.011 + i(0.001 \pm 0.012)$
3	3	$0.009 \pm 0.005 + i(-0.006 \pm 0.006)$	$0.005 \pm 0.012 + i(0.037 \pm 0.012)$
4	0	0.009 ± 0.007	-0.013 ± 0.014
4	2	$0.004 \pm 0.005 + i(0.006 \pm 0.005)$	$-0.015 \pm 0.011 + i(0.002 \pm 0.010)$
4	4	$0.004 \pm 0.005 + i(0.011 \pm 0.005)$	$0.009 \pm 0.010 + i(-0.006 \pm 0.010)$
5	1	$0.007 \pm 0.005 + i(0.001 \pm 0.005)$	$0.004 \pm 0.009 + i(0.008 \pm 0.009)$
5	3	$-0.008 \pm 0.004 + i(-0.001 \pm 0.005)$	$-0.005 \pm 0.010 + i(-0.010 \pm 0.009)$
5	5	$-0.001 \pm 0.005 + i(-0.008 \pm 0.005)$	$0.010 \pm 0.009 + i(0.000 \pm 0.009)$

may be determined from the relations

$$W_{K^{-M}} = (-1)^M W_{K^M},$$

$$W_{K^M} = 0 \quad \text{if } (K+M) \text{ is odd.}$$

The relationship between these coefficients and the partial-wave amplitudes is not very transparent.¹¹⁻¹⁴ Only qualitative conclusions about the contributing angular momentum amplitudes may be inferred from the values of these coefficients. It can be seen from Table IV, giving the confidence levels that particular

moments are zero, that all W_{K^M} with $K=1, 2$ are nonzero. The W_1^1 coefficient is a sum of products of initial-state angular momentum wave amplitudes, with each term a product of opposite-parity amplitudes. Thus the inelastic reactions proceed from at least two initial-state states of opposite parity.¹⁷ Only angular momentum states with $J \geq L + \frac{1}{2}$ contribute to the W_{2L^M} moments. The maximum total angular momentum with significant amplitude may be obtained

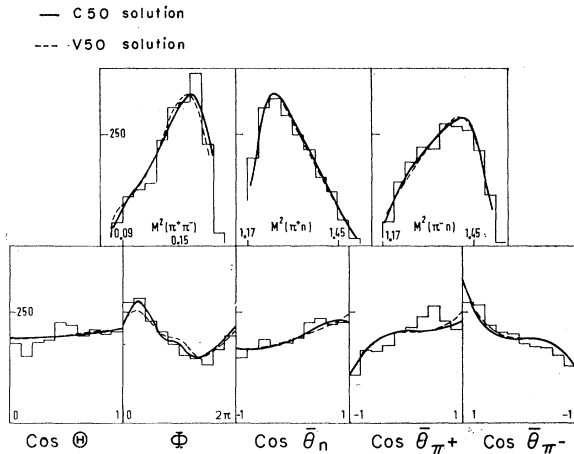


FIG. 11. Angular distributions and $(\text{mass})^2$ spectra for $\pi^-p \rightarrow \pi^+\pi^-n$ at 505 MeV/c with "cube" and "Veneziano" fits.

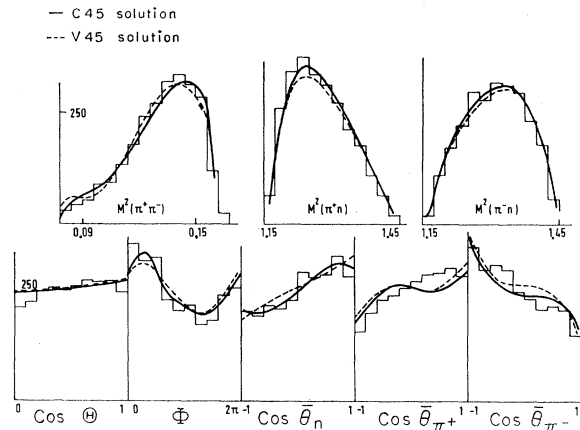


FIG. 12. Angular distributions and $(\text{mass})^2$ spectra for $\pi^-p \rightarrow \pi^+\pi^-n$ at 456 MeV/c with "cube" and "Veneziano" fits.

¹⁷ It is not possible to determine the parity of a particular wave without polarization information or the use of a dynamical model. This point has sometimes been neglected.

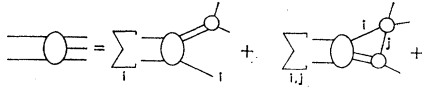


FIG. 13. Expansion of a $2 \rightarrow 3$ body amplitude into isobar terms and triangle graphs.

directly from the knowledge of the maximum value of K in the spherical harmonic series. As can be seen from Tables III and IV, only those moments with $K \leq 4$ are significantly different from zero. There is therefore no need for both $D_{5/2}$ and $F_{5/2}$ waves. In subsequent analysis we have considered only waves of $J \leq \frac{3}{2}$.

IV. ISOBAR MODEL

A. General Remarks

Because of the low c.m. energy, the natural formalism to consider is an s -channel partial-wave analysis. The (mass)² spectra suggest that the $\pi^+\pi^-n$ final state is dominated by Δ resonance production, and perhaps a $\pi\pi$ interaction. This situation suggests application of an "isobar model." If the two-particle to two-particle amplitude is dominated by resonances (this is referred to as the "separable" approximation, since the transition amplitudes separate into a factor depending on the initial state only and one depending on the final state only), then the two-to-three-particle amplitude can be expanded in a series, which can be written diagrammatically as in Fig. 13. If one curtails the series at the first term, one has the "isobar model."¹⁸⁻²¹

The second-order "rescattering" graphs are usually small,²² except at low energies. Anisovich and Dakhno²³ have suggested that the high-mass $\pi^+\pi^-$ peak in $\pi^+\pi^-n$ is due to destructive interference of the rescattering and isobar terms at low $\pi^+\pi^-$ masses. Anisovich *et al.*²⁴

TABLE IV. Confidence levels for the hypothesis that all W_{KM} moments of a given K are zero within the statistics.

K		1	2	3	4	5
$\pi^+\pi^-n$	456	<0.0001	0.006	0.12	0.08	0.60
	505	<0.0001	0.04	0.15	0.15	0.40
	552	<0.0001	<0.0001	0.20	0.10	0.35
$\pi^-\pi^0p$	552	0.015	0.02	0.03	0.50	0.75

¹⁸ L. D. Faddeev, Zh. Eksperim. i Teor. Fiz. **39**, 1459 (1960) [Soviet Phys. JETP **12**, 1014 (1961)].

¹⁹ M. Froissart and R. Omnes, in *High Energy Physics*, edited by C. De Witt and M. Jacob (Gordon and Breach, New York, 1966), pp. 177 ff.

²⁰ C. Lovelace, Phys. Rev. **135**, B1225 (1964).

²¹ D. Z. Freedman, C. Lovelace, and J. M. Namyslowski, Nuovo Cimento **53**, 258 (1966).

²² I. J. R. Aitchison, Nuovo Cimento **51A**, 249 (1967); **51A**, 272 (1967); I. J. R. Aitchison, Phys. Rev. **133**, B1257 (1964).

²³ V. V. Anisovich and L. G. Dakhno, Phys. Letters **10**, 221 (1964).

²⁴ V. V. Anisovich, E. M. Levin, A. K. Likhoded, and Y. G. Stroganov, Yadern. Fiz. **8**, 583 (1969) [Soviet J. Nucl. Phys. **8**, 339 (1969)].

have fitted the data of Batusov *et al.*²⁵ with a series of terms, which include a $\pi\pi$ rescattering vertex but not $\pi\pi$ isobar production. In this paper we fit the data using only the first-order (isobar) terms. Any residual discrepancies between the isobar model predictions and the data may be due to the rescattering terms.

In the formulation of the model used here, all angular momentum, isospin, and interference effects are taken into account. Such models have been described by Olsson and Yodh,¹⁰ Deler and Valladas,¹⁵ and Namyslowski, Razmi, and Roberts.²⁶ The formalism used here is conceptually similar to that of Deler and Valladas, and so details of the derivation are not given.

B. Formulation of Isobar Model

The production of an isobar of particles 1 and 2, with spin j_{12} and orbital angular momentum l_{12} , is described in an angular momentum basis $|(12)3\rangle$.^{26,27} We quantize l_{12} , the relative angular momentum of 1 and 2, j_{12} , the total angular momentum of 1 and 2, L_3' , the relative angular momentum of 3 and the (12) system in the over-all c.m. system, and J , the total angular momentum.²⁸

The matrix element for production of a (12) isobar involves only one value of j_{12} and l_{12} .

Production of a (13) isobar is described in terms of $j_{13}l_{13}L_2'J$. This basis is not orthogonal to $j_{12}l_{12}L_3'J$. We are therefore "double counting" to some extent. The advantage of this scheme is that we simply make use of the isotopic spin relations between Δ^- production in the $|(\pi^-n)\pi^+\rangle$ basis and Δ^+ production in the $|(\pi^+n)\pi^-\rangle$ basis. The three-body production amplitude is then a sum of amplitudes for the three processes

$$\begin{aligned} \pi N \rightarrow \pi_2 \Delta_1, \quad \Delta_1 \rightarrow \pi_1 N; \quad \pi N \rightarrow \pi_1 \Delta_2, \quad \Delta_2 \rightarrow \pi_2 N; \\ \pi N \rightarrow N \sigma, \quad \sigma \rightarrow \pi \pi. \end{aligned}$$

Including all kinematic factors within the definition of the matrix element, the differential cross section is

$$\begin{aligned} \frac{\partial^4 \sigma}{\partial m_{12}^2 \partial m_{23}^2 \partial \cos \Theta \partial \Phi} = \frac{1}{2} \sum_{M M_s} \left| \sum_{J L L', I} [T_I^{J L L'}(\pi \Delta_1) \right. \\ \left. + T_I^{J L L'}(\pi \Delta_2)] + \sum_{J L L'} T^{J L L'}(\sigma N) \right|^2, \end{aligned}$$

where the sum over final nucleon spin M_s and average over initial spin M are indicated. The axis of quantization in each case is the z axis defined in Sec. II C. Each

²⁵ Yu. A. Batusov *et al.* Zh. Eksperim. i Teor. Fiz. **43**, 2015 (1962) [Soviet Phys. JETP **16**, 1422 (1963)].

²⁶ J. M. Namyslowski, M. S. K. Razmi, and R. G. Roberts, Imperial College, London, Report No. ICTP/65/20 (unpublished); Phys. Rev. **157**, 1328 (1967).

²⁷ G. Wick, Ann. Phys. (N. Y.) **18**, 65 (1962).

²⁸ This base is not Lorentz invariant. However, H. P. Stapp [Phys. Rev. **103**, 425 (1956)] has shown that the most important relativistic effect is a rotation of the polarization of the isobar when a Lorentz transformation is made from the c.m. frame for production to the c.m. frame for decay. This angle is typically less than 3° at these energies. One therefore neglects the effect.

amplitude is to be understood as dependent upon M and M_s , though not explicitly indicated by the notation. Here $T_I^{JLL'}$ are the partial-wave projections of the T matrix for Δ production in the state with total isotropic spin I . J and L' have the meanings above and L is the relative angular momentum in the initial state. $T^{JLL'}$ are the amplitudes for production of an $I=0$, $J=0$ dipion isobar, σ (see Sec. IV D) in the $I=\frac{1}{2}$ state only.

C. $\pi\Delta$ Channel

We write the isospin decomposition of $\pi^-p \rightarrow \pi\Delta_1$

$$T_I^{JLL'}(\pi\Delta_1) = C_{q_\pi q_N I_3}^{1\frac{1}{2}} I C_{q_1 q_N' q_1'}^{1\frac{1}{2}} I C_{q_2 q_1' I_3}^{1\frac{1}{2}} I T_I^{JLL'}(\pi\Delta),$$

where q_π , q_N , q_N' , and q_1' are the third components of isotopic spin of the incident π^- , initial and final nucleons and Δ_1 ; q_1 and q_2 are the charges of final-state pions 1 and 2, and Δ_1 is made of π_1 and N , with $q_1' = q_1 + q_N$. The constants C_{abc}^{ABC} are Clebsch-Gordan coefficients.

Factors containing the angular dependence of the $T_I^{JLL'}(\pi\Delta)$ are separated out as follows:

$$T_{IMM_s}^{JLL'}(\pi\Delta) = T_I^{JLL'}(s^{1/2}, m_\Delta) f_{MM_s}^{JLL'}(\Theta, \Phi, \phi_1, \theta^*),$$

where the suffices M and M_s have been reinserted. $T_I^{JLL'}(s^{1/2}, m_\Delta)$ is a reduced matrix element of the Breit-Wigner form for Δ final-state interaction together with an angular momentum barrier for Δ production at total c.m. energy $s^{1/2}$.

The form used here is^{29,30}

$$T_I^{JLL'}(s^{1/2}, m_\Delta) \propto p^{L'} \frac{\omega_0 \Gamma_0 (q/q_0)}{\omega^2 - \omega_0^2 + i\omega_0 \Gamma_0 (q/q_0)^2},$$

where p is the momentum of the Δ in the c.m. system and q is the momentum of the final π and N in the Δ rest frame.

The numerical factors are

$$\begin{aligned} \omega_0 &= 1236 \text{ MeV}, \\ \Gamma_0 &= 120 \text{ MeV}, \\ q_0 &= 225 \text{ MeV}/c. \end{aligned}$$

Only the proportionality sign was kept and kinematic factors depending only on s were not retained since we made one-energy fits and normalization was taken from experiment.

The angular dependence is in the term

$$f_{MM_s}^{JLL'}(\Theta, \Phi, \phi_1, \theta^*),$$

where Θ and Φ are defined above. In this section the x axis is arbitrary except that it must be in the final-state plane. Other angles occurring are the following: ϕ_1 is the azimuthal angle of Δ in the c.m. system, and θ^* is

²⁹ K. M. Watson, Phys. Rev. **85**, 852 (1952).

³⁰ J. D. Jackson, CERN Report No. CERN/TH 416, 1964 (unpublished).

TABLE V. Δ production from $M=\frac{1}{2}$. The arguments of the spherical harmonic are Θ, Φ throughout.

Wave	M_s	Amplitude
SD1	$\frac{1}{2}$	0
	$-\frac{1}{2}$	$-\frac{1}{4}\sqrt{2}Y_{00}^*e^{i\phi_1}(2\cos\theta^*-i\sin\theta^*)$
PP1	$\frac{1}{2}$	$\frac{1}{2}\sqrt{6}Y_{10}^*(2\cos\theta^*+i\sin\theta^*)$
	$-\frac{1}{2}$	$\frac{1}{6}\sqrt{3}Y_{1-1}^*(2\cos\theta^*-i\sin\theta^*)$
PP3	$\frac{1}{2}$	$(1/2\sqrt{30})Y_{10}^*(\cos\theta^*+5i\sin\theta^*)$
	$-\frac{1}{2}$	$(1/4\sqrt{15})[3Y_{11}^*e^{2i\phi_1}(\cos\theta^*+i\sin\theta^*) + Y_{1-1}^*(5i\sin\theta^*-\cos\theta^*)]$
DS3	$\frac{1}{2}$	$\frac{1}{4}(\sqrt{\frac{3}{2}})[Y_{21}^*e^{i\phi_1}(\cos\theta^*+i\sin\theta^*) + Y_{2-1}^*e^{-i\phi_1}(i\sin\theta^*-\cos\theta^*)]$
	$-\frac{1}{2}$	$\frac{1}{4}(\sqrt{\frac{3}{2}})[(\sqrt{\frac{3}{2}})Y_{20}^*e^{i\phi_1}(\cos\theta^*+i\sin\theta^*) + 2Y_{2-2}^*e^{-i\phi_1}(i\sin\theta^*-\cos\theta^*)]$
DD3	$\frac{1}{2}$	$\frac{1}{4}(\frac{3}{2})(-Y_{21}^*\cos\theta^*+Y_{2-1}^*e^{-i\phi_1}[2i\sin\theta^*+\cos\theta^*])$
	$-\frac{1}{2}$	$\frac{3}{8}[(\sqrt{1/6})Y_{20}^*e^{i\phi_1}(-\cos\theta^*+2i\sin\theta^*) + (\sqrt{3/8})Y_{2-2}^*\cos\theta^*e^{-i\phi_1}]$
DD5	$\frac{1}{2}$	$(1/2\sqrt{35})[-Y_{21}^*e^{i\phi_1}(\cos\theta^*+5i\sin\theta^*) + Y_{2-1}^*e^{-i\phi_1}(2i\sin\theta^*+\cos\theta^*)]$
	$-\frac{1}{2}$	$(1/4\sqrt{35})[Y_{2-2}^*e^{-i\phi_1}(5i\sin\theta^*-\cos\theta^*) - 5Y_{23}^*e^{3i\phi_1}(\cos\theta^*+i\sin\theta^*) + (\sqrt{6})Y_{20}^*e^{i\phi_1}(\cos\theta^*-2i\sin\theta^*)]$
FP5	$\frac{1}{2}$	$\frac{1}{4}(\sqrt{3/7})[Y_{32}^*e^{2i\phi_1}(\cos\theta^*+i\sin\theta^*) + Y_{3-2}^*e^{-2i\phi_1}(\cos\theta^*-i\sin\theta^*)] - \frac{3}{2}(1/\sqrt{70})Y_{30}^*\cos\theta^*$
	$-\frac{1}{2}$	$\frac{1}{2}(\sqrt{3/70})[Y_{31}^*e^{2i\phi_1}(i\sin\theta^*+\cos\theta^*) - 2Y_{3-1}^*\cos\theta^*] + \frac{3}{2}(\sqrt{2/7})Y_{3-3}^*e^{-2i\phi_1}(\cos\theta^*-i\sin\theta^*)$

the angle of the pion in the Δ rest frame defined as $\theta^*=0$ with the two pions travelling in opposite directions in this frame. These variables depend on $M_{\pi\pi}{}^2$, $M_{\pi N}{}^2$, Θ , and Φ .

Suppressing some coefficients,

$$\begin{aligned} f_{MM_s}^{JLL'} &= \sum_{MLM_s'm} C_{MM_s(ML+M)}^{L\frac{1}{2}J} \\ &\times C_{(ML+M-M_s')M_s'(ML+M)}^{L'\frac{1}{2}J} C_{(M_s'-M_s)M_sM_s'}^{1\frac{1}{2}} \\ &\times Y_{LM}^*(\Theta, \Phi) Y_{L'(ML+M-M_s')}(\frac{1}{2}\pi, \phi_1) \\ &\times Y_{1m}(\theta^*, 0) i^m d_{m(M_s'-M_s)}^{1\frac{1}{2}}(\frac{1}{2}\pi) e^{i\phi_1(M_s'-M_s)}. \end{aligned}$$

In Table V the explicit forms for $M=\frac{1}{2}$ for various partial waves are given. The notation used in labelling the partial waves is $LL'(2J)(2I)$; if $I=\frac{1}{2}$, the last term is omitted. Waves permitted by angular momentum and parity selection rules are then

$$SD1, PP1, PP3, DS3, DD3, DD5, FP5$$

and higher waves, for $I=\frac{1}{2}$ and $I=\frac{3}{2}$. From this angle-dependent formula, the following relations are deduced:

$$L'+M_L+M-M_s'$$

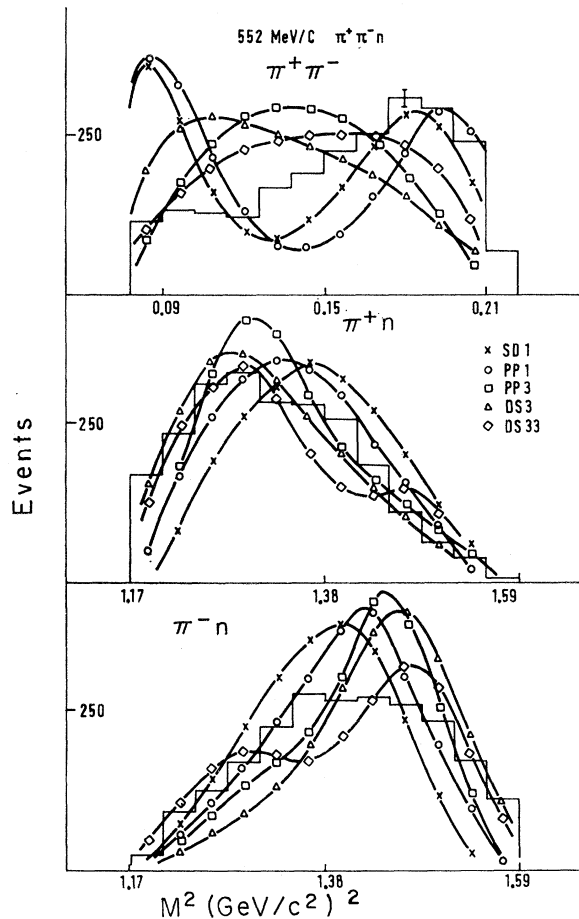


FIG. 14. (Mass)² spectra from $\pi\Delta$ production in pure angular momentum waves for $\pi^+\pi^-n$ at 552 MeV/c.

is even,

$$M_S' = M_S \pm 1,$$

$$f_{MM_S}^{JLL'}(\Theta, \Phi, \phi_1, \theta^*) = [f_{-M-M_S}^{JLL'}(\Theta, \Phi, \phi_1, \theta^*)]^* (-1)^{M-M_S}.$$

Further, waves differing in total angular momentum or parity do not interfere in the Dalitz plot or its projections. Effective-mass distributions depend strongly on the form of the angular dependence of the decay distribution. For instance, because of the $(1 + \cos^2\theta)$ decay angular distribution of the isobar, the spin- $\frac{1}{2}$ waves give $\pi^+\pi^-$ (mass)² spectra sharply peaked at both high and low ends. In Fig. 14 the (mass)² spectra due to various Δ production waves are shown for 552-MeV/c $\pi^+\pi^-n$.

D. $N\sigma$ Channel

1. $\pi\pi$ S-Wave Phase Shift δ_{00}

The $\pi\pi$ interaction, σ , is described in terms of the $I=J=0$ $\pi\pi$ phase shift δ_{00} . There is, unfortunately, no reliable experimental information on $\pi\pi$ phase shifts

below 500 MeV. Indeed, experimentally, $\pi\pi$ phase shifts can be measured only in situations with one or both π 's off the mass shell. The method of greatest success has been the study of the reaction $\pi^-p \rightarrow \pi\pi N$ and $\pi\pi\Delta$, using Chew-Low extrapolations to isolate the one-pion-exchange contributions.^{31,32} This work has indicated that δ_{00} passes near 90° near 720 MeV total $\pi\pi$ energy. It is a matter of interest to determine the explicit dependence on energy,^{32,33} particularly near threshold where some theoretical calculations are available. However, at low $\pi\pi$ masses there are so few data that no conclusions can be drawn.³⁴ The same defect holds in the theoretically cleaner study of K_{e4} decay.³⁵ Other methods such as the study of $K \rightarrow 3\pi$,³⁶ and $\eta \rightarrow 3\pi$ decay³⁷ and the rates for $K\pi 2$ decay,³⁸ are of ambiguous interpretation.

Some direction provided by theoretical arguments was followed. The work of Morgan and Shaw³⁹ is of particular interest because it relates the $\pi\pi$ phase shifts below 500 MeV to the width of the resonance at 720 MeV. Two extreme cases are distinguished, viz., a resonance width of about 200 MeV gives δ_{00} small

³¹ J. P. Baton, G. Laurens, and J. Reignier, Nucl. Phys. B3, 349 (1967).

³² L. J. Gutay, D. D. Carmony, P. L. Csonka, F. J. Loeffler, and F. T. Meiere, Purdue University Report No. C00-1428-65 (unpublished); G. L. Kane and M. Ross, Phys. Rev. 177, 2353 (1969); P. B. Johnson, J. A. Poirier, N. N. Biswas, N. M. Cason, T. H. Groves, V. P. Kenney, J. T. McGahan, W. D. Shephard, L. J. Gutay, J. H. Campbell, R. L. Elsner, F. J. Loeffler, R. E. Peters, R. J. Sahni, W. L. Yen, L. Derado, and Z. G. T. Guragossian, *ibid.* 176, 1651 (1968); L. J. Gutay, in Proceedings of the Argonne Conference on $\pi\pi$ and $K\pi$ Interactions, 1969, p. 241 ff (unpublished); E. Colton and P. E. Schlein, *ibid.*, p. 1 ff; E. Malamud and P. E. Schlein, *ibid.*, p. 93 ff; W. D. Walker, J. Carroll, A. Garfinkel, and B. Y. Oh, Phys. Rev. Letters 18, 630 (1967).

³³ G. A. Smith and R. J. Manning, Phys. Rev. 171, 1399 (1968); I. F. Corbett, C. J. S. Damerell, N. Middlemas, D. Newton, A. B. Clegg, W. S. C. Williams, and A. S. Carroll, Phys. Rev. 156, 1451 (1967).

³⁴ N. N. Biswas, N. M. Cason, P. B. Johnson, V. P. Kenney, J. A. Poirier, W. D. Shephard, and R. Torgerson, Phys. Letters 27B, 513 (1968).

³⁵ F. A. Berends, A. Donnachie, and G. C. Oades, Nucl. Phys. B3, 569 (1967); R. P. Ely, G. Gidal, V. Hagopian, G. E. Kalmus, K. Billing, F. W. Bullock, M. J. Esten, M. Govan, C. Henderson, W. L. Knight, F. R. Stannard, O. Treutler, U. Camerini, D. Cline, W. F. Fry, H. Haggerty, R. H. March, and W. J. Singleton, Phys. Rev. 180, 1319 (1969); A. Pais and S. B. Treiman, *ibid.* 168, 1858 (1968); N. Cabibbo and A. Maksymowicz, *ibid.* 137, B438 (1965); 168, 1926(E) (1968).

³⁶ D. Davison, R. Bacastow, W. H. Barkas, D. A. Evans, S.-Y. Fong, L. E. Porter, R. T. Poe, and D. Greiner, Phys. Rev. 180, 1333 (1969); R. N. Chaudhuri, *ibid.* 175, 2066 (1968); L. M. Brown and P. Singer, *ibid.* 133, B812 (1964); A. N. Mitra and S. Ray, *ibid.* 135, B146 (1964); N. N. Khuri and S. B. Treiman, *ibid.* 119, 1115 (1960); V. N. Gribov, Zh. Eksperim. i Teor. Fiz. 41, 1221 (1961) [Soviet Phys. JETP 14, 871 (1962)]; V. V. Anisovich, Zh. Eksperim. i Teor. Fiz. 17, 1072 (1963); 20, 161 (1965) [Soviet Phys. JETP 44, 1593 (1963); 47, 240 (1964)]; M. Baldo-Ceolin *et al.*, Nuovo Cimento 6, 84 (1957); S. McKenna *et al.*, *ibid.* 10, 763 (1958); G. Kalmus *et al.*, Phys. Rev. Letters 13, 99 (1964).

³⁷ A. Larribe, A. Leveque, A. Muller, E. Pauli, D. Revel, B. Tallini, P. Litchfield, L. K. Rangan, A. M. Segar, J. R. Smith, P. J. Finney, C. M. Fisher, and E. Pickup, Phys. Letters 23, 600 (1966); F. S. Crawford, R. A. Grossman, L. J. Lloyd, L. R. Price, and E. C. Fowler, Phys. Rev. Letters, 11, 564 (1963).

³⁸ T. D. Lee and C. S. Wu, Ann. Rev. Nucl. Sci. 16, 528 (1966).

³⁹ D. Morgan and G. Shaw, Nucl. Phys. B10, 261 (1969).

(<15°) up to 500 MeV and a width about 800 MeV gives δ_{00} rising smoothly from threshold up to 50° at 500 MeV. The results of a recent calculation by Lovelace using an amplitude of the Veneziano type gives $\pi\pi$ phase shifts of this second form (with scattering length $a_{00} = 0.29M_\pi^{-1}$).^{40,41}

Two forms of δ_{00} were used as $\pi\pi$ final-state interaction factors in this work. First, a form having zero scattering length, increasing approximately as q^3 from threshold [called here the C (cube) form] and secondly the Veneziano-Lovelace (V) form of δ_{00} . Both are referred to as a σ state without implying a low-mass $I=J=0$ resonance. Figure 15 shows the energy dependence of the two forms used. ρ -meson production ($I=J=1$ $\pi\pi$ pair) was not considered. At the $\pi\pi$ masses accessible in this experiment ($\lesssim 450$ MeV/c²), it is now believed^{39,40} that the p -wave phase shifts are small (below 5° at 500 MeV). A second, *post facto*, justification in ignoring ρ production is that one can fit the $\pi^-\pi^0p$ data, to which the σ does not contribute, with $\pi\Delta$ production alone (see Sec. V).

The Watson final-state interaction³⁰ factor in the production matrix element was used. That is,

$$T \propto p^{L'} q^{-1} (\cot \delta_{00} - i)^{-1},$$

where L' is the relative angular momentum of σ and N , p is their relative momentum, and q is the π momentum in the dipion rest frame.

2. Isobar Formalism for $N\sigma$

In a manner similar to that for the $\pi\Delta$ process (Sec. IV C), we write the production amplitude for the

$$\pi N \rightarrow \sigma N, \quad \sigma \rightarrow \pi\pi$$

TABLE VI. σ production from $M = \frac{1}{2}$. The arguments of the spherical harmonics are Θ, Φ throughout. The x axis is along the path of the outgoing nucleon.

Wave	M_S	Amplitude
SP1	$\frac{1}{2}$	0
	$-\frac{1}{2}$	$\frac{1}{2} Y_{00}^*$
PS1	$\frac{1}{2}$	$-\frac{1}{2}\sqrt{3} Y_{10}^*$
	$-\frac{1}{2}$	$-(\frac{1}{2}\sqrt{6}) Y_{1-1}^*$
PD3	$\frac{1}{2}$	$(\frac{1}{2}\sqrt{6}) Y_{10}^*$
	$-\frac{1}{2}$	$\frac{1}{2}\sqrt{3}(3Y_{11}^* - Y_{1-1}^*)$
DP3	$\frac{1}{2}$	$\frac{1}{4}(\sqrt{\frac{3}{2}})(Y_{2-1}^* - Y_{21}^*)$
	$-\frac{1}{2}$	$\frac{1}{4}(\sqrt{\frac{3}{2}})[2Y_{2-2}^* - (\sqrt{\frac{3}{2}})Y_{20}^*]$
DF5	$\frac{1}{2}$	$\frac{1}{4}(\sqrt{\frac{3}{2}})(Y_{21}^* - Y_{2-1}^*)$
	$-\frac{1}{2}$	$\frac{1}{8}(1/\sqrt{15})[Y_{22}^* 5\sqrt{6} - 6Y_{20}^* + (\sqrt{6})Y_{2-2}^*]$
FD5	$\frac{1}{2}$	$-\frac{1}{4}(\sqrt{5/14})(Y_{32}^* + Y_{3-2}^*) + \frac{1}{4}(\sqrt{3/7})Y_{30}^*$
	$-\frac{1}{2}$	$\frac{1}{4}(1/\sqrt{7})[-Y_{31}^* + 2Y_{3-1}^* - (\sqrt{15})Y_{3-3}^*]$

⁴⁰ C. Lovelace, in Proceedings of the Argonne Conference on $\pi\pi$ and $K\pi$ Interactions, 1969, p. 562 (unpublished); CERN Report No. CERN/TH 1041, 1969 (unpublished).

⁴¹ F. Wagner, Nuovo Cimento **64A**, 189 (1969).

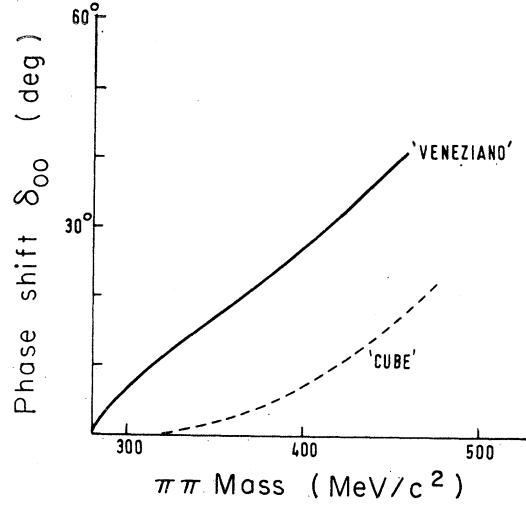


FIG. 15. Mass dependence of $\pi\pi$ scattering phase shift δ_{00} for the "cube" and "Veneziano" forms.

mechanism:

$$T_{MM_S}^{JLL'}(\sigma N) = T^{JLL'}(s^{1/2}, m_\sigma) f_{MM_S}^{JLL'}(\Theta, \Phi),$$

$$f_{MM_S}^{JLL'}(\Theta, \Phi) = \sum_{M_L} C_{MLMM_S}^{L'J} Y_{LM_L}^*(\Theta, \Phi)$$

$$\times Y_{L'M'L}(\frac{1}{2}\pi, \pi) \frac{1}{(4\pi)^{1/2}} C_{ML'M_S M_J}^{L'J},$$

with

$$M_L' = M_J - M_S, \quad M_J = M + M_L.$$

The x axis in this equation is along the neutron direction.

Table VI gives explicit forms for the allowed partial-wave amplitudes, only from states of $I = \frac{1}{2}$,

$$SP1, \quad PS1, \quad PD3, \quad DP3, \quad DF5, \quad FD5.$$

V. DETERMINATION OF PARTIAL-WAVE AMPLITUDES

A. Fitting Procedures

Distributions in eight variables, the three effective-mass-squared combinations, $\cos\Theta, \Phi$, and three production angles, were fitted. Theoretical distributions in these variables were obtained, using Monte Carlo techniques, for particular values of the complex amplitudes multiplying the factors discussed above, for the following set of partial waves:

$$\pi\Delta: \quad SD1, \quad PP1, \quad PP3, \quad DS3, \quad \text{and} \quad DS33^{42};$$

$$\sigma N: \quad SP1, \quad PS1.$$

⁴² This $I = \frac{3}{2}$ wave was included since the work of Bowler and Cashmore (Ref. 16) on π^+p inelastic reactions at 600–800 MeV/c indicates that this is the dominant $I = \frac{3}{2}$ $\pi N \rightarrow \pi\Delta$ wave and that all others are small. In $I = \frac{1}{2}$ $\pi\Delta$ production in $\pi^-p\pi^0$, the $\Delta^+\pi^-$ and $\Delta^0\pi^0$ amplitudes are equal and opposite, so that distributions should be invariant under an interchange of π^- and π^0 , whereas experimentally there are significant differences in M^2 (πp) and $\cos\theta_r$ distributions. (See Figs. 8 and 9.)

TABLE VII. Predicted branching ratios $\sigma(\pi^+\pi^-n)/\sigma(\pi^-\pi^0p)$ at 552 MeV/c.

Partial wave	Branching ratio
<i>SD1</i>	2.33
<i>PP1</i>	3.70
<i>PP3</i>	1.32
<i>DS3</i>	2.97
<i>DS33</i>	1.54
Experiment	4.22 ± 0.21

Best-fit values of the amplitudes and phases were obtained by minimizing

$$\chi^2 = \sum \left[\frac{N_{\text{expt}} - N_{\text{theory}}}{\Delta N_{\text{theory}}} \right]^2,$$

with the sum taken over all bins of the eight histograms. The theoretical distributions were normalized to the total number of events so that absolute cross sections were not included as data to be fitted.

In making simultaneous fits to the $\pi^+\pi^-n$ and $\pi^-\pi^0p$ distributions at 552 MeV/c, the number of $\pi^-\pi^0p$ events was arbitrarily increased by a factor 4 to give the two sets of data approximately equal statistical weight.⁴³

B. Results of Fit with $\pi\Delta$ Channel Only

Both $\pi\Delta$ and σN channels were shown to be necessary because of the poor fits with predictions of the isobar model without the σ intermediate state. A fit with only $\pi\Delta$ channel amplitudes was unsuccessful in two important respects. The high-mass $\pi^+\pi^-$ enhancement in the $\pi^+\pi^-n$ final state was not reproduced. No combination of partial waves yielded a high-mass peaking without at the same time requiring a low-mass peak (see Fig. 14 and the remarks at the close of Sec. IV C). The absence of interference, in the mass spectra, between waves of different J or P enables one to make this statement with confidence. Further, the branching ratio $\sigma(\pi^+\pi^-n)/\sigma(\pi^-\pi^0p)$ at 552 MeV/c is not given correctly. The experimental ratio is significantly larger than that obtainable from any partial wave, as shown

in Table VII. No mixture of waves can produce the observed cross sections' ratio.

It is clear that some mechanism other than $\pi\Delta$ production contributes substantially to the $\pi^+\pi^-n$ state and causes the distribution in the $\pi^+\pi^-$ effective-mass spectrum. Satisfactory fits were obtained to the $\pi^-\pi^0p$ data, however, with the $\pi\Delta$ mechanism alone. Thus it is indicated that there is no significant effect due to $I=1, J=1$ ρ -meson production, so that the significant $\pi\pi$ final-state interaction is likely in the $I=0$ state.

C. Results of Fit with $\pi\Delta$ and σN Channels

A sequence of fits to the data with the predictions of the isobar model following the procedure outlined above was made with both the C and V forms of $\pi\pi$ phase shifts. This included:

- a fit to both final states at 552 MeV/c;
- using the results of these fits as starting values, a fit to each data set individually.

This procedure should find in case (b) a solution similar to that in case (a), if it exists. Questions of uniqueness have been evaded.

In Figs. 7-12 the theoretical predictions using best-fit parameters are shown superimposed on the experimental histograms and in Table VIII the partial-wave amplitudes and χ^2 per degree of freedom of the fits are given.

The normalization is to one event in $\pi^+\pi^-n$ at each energy (i.e., $a_{P3}=1$ if the reaction proceeds entirely through *PP3*, etc.).

Using the designation of a partial wave to denote its amplitude, the parameters obtained in the fits are

$$\begin{aligned} a_{P3} &= PP3, \\ a_{D3} &= DS3 + DS33, \\ p_{D13} &= DS3/(DS3 + DS33), \\ a_{S1} &= (SD1 + SP1), \\ p_{SD1} &= SD1/(SD1 + SP1), \\ a_{P1} &= (PP1 + PS1), \\ p_{PP1} &= PP1/(PP1 + PS1), \end{aligned}$$

TABLE VIII. Partial-wave parameters and χ^2 per degree of freedom.

Fit	χ^2/NDF	a_{P3}	a_{D3}	p_{D13}	a_{S1}	p_{SD1}	a_{P1}	p_{PP1}
<i>C</i>	2.4	0.28 ± 0.09	0.74 ± 0.13	0.86 ± 0.17	0.51 ± 0.21	0.36 ± 0.16	0.71 ± 0.12	0.22 ± 0.21
<i>C55</i>	2.1	0.27 ± 0.07	0.72 ± 0.05	0.58 ± 0.11	0.62 ± 0.10	0.28 ± 0.10	0.76 ± 0.04	0.32 ± 0.19
<i>Cπ^0</i>	1.2	0.29 ± 0.08	0.93 ± 0.29	0.68 ± 0.09	0.15 ± 0.11	1	0.32 ± 0.19	1
<i>V</i>	2.5	0.19 ± 0.10	0.76 ± 0.09	0.70 ± 0.09	0.34 ± 0.20	0.35 ± 0.36	1.00 ± 0.10	0.50 ± 0.10
<i>V55</i>	2.8	0.23 ± 0.07	0.64 ± 0.04	0.55 ± 0.12	0.40 ± 0.08	0.22 ± 0.15	1.01 ± 0.05	0.48 ± 0.03
<i>Vπ^0</i>	1.4	0.32 ± 0.05	0.80 ± 0.12	0.81 ± 0.08	0.16 ± 0.11	1	0.02 ± 0.01	1
<i>C50</i>	2.0	0.38 ± 0.07	0.57 ± 0.06	0.53 ± 0.16	0.47 ± 0.11	0.21 ± 0.13	0.78 ± 0.05	0.25 ± 0.09
<i>V50</i>	2.6	0.34 ± 0.06	0.49 ± 0.06	0.60 ± 0.16	0.34 ± 0.09	0.25 ± 0.20	1.03 ± 0.04	0.46 ± 0.04
<i>C45</i>	1.7	0.35 ± 0.06	0.50 ± 0.06	0.41 ± 0.14	0.47 ± 0.10	0.23 ± 0.10	0.84 ± 0.04	0.21 ± 0.07
<i>V45</i>	2.4	0.21 ± 0.07	0.40 ± 0.05	0.58 ± 0.16	0.30 ± 0.11	0.39 ± 0.17	1.12 ± 0.04	0.43 ± 0.03

⁴³ This is not a true χ^2 because we have taken eight projections of a four-dimensional space. (We make only one-energy fits.) However, there is clearly more information in a four-dimensional space than in four orthogonal projections of it, so that no serious redundancy is introduced by attempting to fit all the distributions.

FIG. 16. Incident momentum dependence of the inelasticity $(1-\eta^2)^{\frac{1}{2}}$ for S_{11} , P_{11} , and P_{13} partial waves inferred from this work and the elastic phase-shift analyses of Refs. 8 and 47.

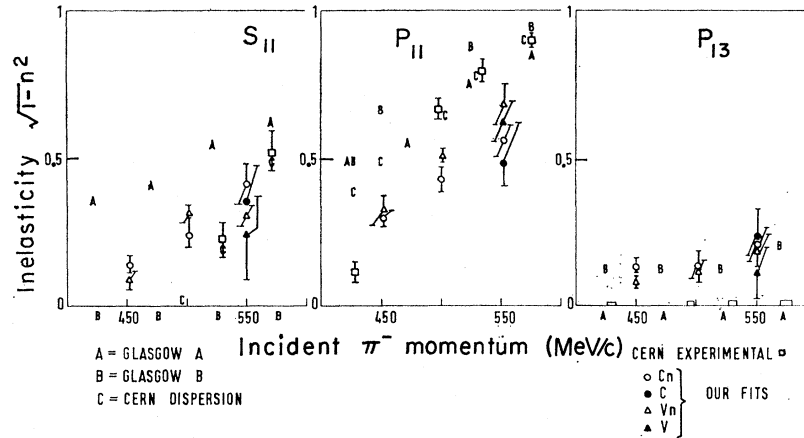
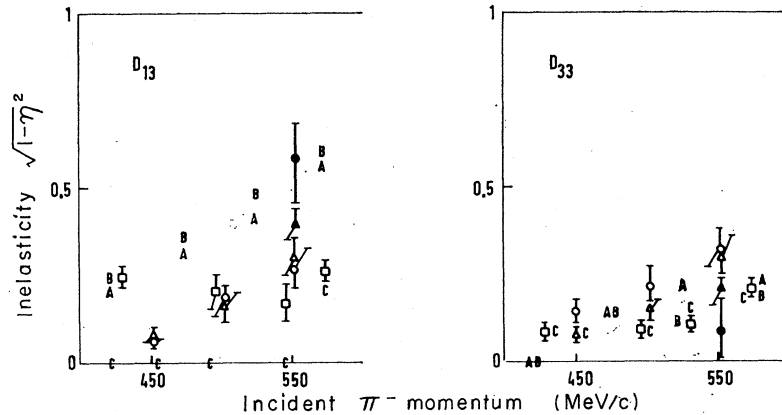


FIG. 17. Incident-momentum dependence of the inelasticity $(1-\eta^2)^{\frac{1}{2}}$ for D_{13} and D_{33} partial waves inferred from this work and the elastic phase-shift analyses of Refs. 8 and 47.



together with the phases of the various waves. These variables were chosen as they are substantially uncorrelated, so that a simple calculation of the errors suffices.⁴⁴ Since the phases show very little energy dependence, we do not quote them in the table.

The notation used is C and V for simultaneous fits to $\pi^+\pi^-n$ and $\pi^-\pi^0p$ at 552 MeV/c, and $C55$, $C50$, $C45$, and $C\pi^0$ for fits to one data set only.

Examination of the graphs and χ^2 per degree of freedom shows that while all the principal features of the data are accounted for by the model, there are some residual discrepancies, particularly in the angular distributions. The sharp high π^-n mass peak in the theory, but not in the data, is probably due to the neglect of the spread in beam momentum in the Monte Carlo calculation.

⁴⁴ The error on a parameter is defined as the change in that parameter from its value when χ^2 has its minimum which makes an increase in χ^2 to a value having a confidence level one-third that of the best fit. (There is then some ambiguity in the fits to both states simultaneously because the function minimized is not a pure χ^2 .) There are two ways of estimating this change. One can hold all other parameters constant at their best values or can change this parameter to a different value and re-minimize χ^2 as a function of all the other parameters. The second scheme is more closely related to the experimental knowledge of the parameter. In this case the two methods agree to within 15% of their estimates of the errors, indicating that the parameters used are not severely correlated. The errors quoted are calculated by the first method.

In all cases the C fits are better, having smaller χ^2 per degree of freedom, than the V fits. On these grounds one prefers variation of δ_{00} with $\pi\pi$ mass below 500 MeV which is more consistent with a "narrow" resonance (about 200 MeV wide), or with a small scattering length than with a broad one. However, this statement must be taken with some caution. Since the best fit is not a good fit, it is conceivable that a V -type solution with some extra terms might prove superior. The fits to $\pi^-\pi^0p$ alone have good χ^2 per degree of freedom, justifying the neglect of ρ production.

VI. PARTIAL-WAVE INELASTICITIES

Using the fitted amplitudes of Sec. V B and the cross sections of Sec. II B, one can predict the values of $(1-\eta^2)^{1/2}$ for the various πN partial waves. All the inelasticity is via the $\pi\pi N$ channel⁴⁵ and predictions can be made for the unobserved final states ($\pi^0\pi^0n$, $\pi^+\pi^+n$, $\pi^+\pi^0p$) using the isobar model.

The inelastic scattering total cross section is given by

$$\sigma_{\text{inel}} = \frac{\pi}{k^2} \sum_{l,J} (J+\frac{1}{2})(1-\eta_l J^2),$$

⁴⁵ S. U. Chung *et al.*, Phys. Rev. 165, 1491 (1968).

TABLE IX. Values of $(1-\eta^2)^{1/2}$.

	S_{11}	P_{11}	P_{13}	D_{13}	D_{33}
C45	0.14 ± 0.03	0.30 ± 0.03	0.13 ± 0.03	0.07 ± 0.01	0.14 ± 0.03
C50	0.24 ± 0.05	0.43 ± 0.04	0.23 ± 0.04	0.18 ± 0.04	0.21 ± 0.05
C55	0.41 ± 0.07	0.56 ± 0.05	0.21 ± 0.06	0.27 ± 0.05	0.32 ± 0.05
C	0.35 ± 0.13	0.48 ± 0.11	0.23 ± 0.09	0.59 ± 0.11	0.09 ± 0.09
V45	0.09 ± 0.03	0.32 ± 0.05	0.08 ± 0.02	0.08 ± 0.02	0.08 ± 0.02
V50	0.19 ± 0.05	0.51 ± 0.02	0.22 ± 0.03	0.16 ± 0.04	0.15 ± 0.03
V55	0.31 ± 0.03	0.68 ± 0.07	0.19 ± 0.06	0.30 ± 0.06	0.31 ± 0.06
V	0.24 ± 0.14	0.63 ± 0.07	0.13 ± 0.08	0.39 ± 0.05	0.21 ± 0.03
Saclay (530 MeV/c)	0.17	0.58	0.08	0.22	0.36

where $k = \hbar/p$, p is the c.m. momentum, and η is the inelasticity parameter.

Table IX gives the values of $(1-\eta_{lJ}^2)^{1/2}$ for the various partial waves, together with the 530-MeV/c results of the Saclay group⁴⁶ for comparison. Figures 16 and 17 show the energy dependence of $(1-\eta_{lJ}^2)^{1/2}$ from this analysis and from the CERN⁸ experimental and theoretical and the Glasgow⁴⁷ A and B analyses. These results show that inelasticity is not well determined by the elastic phase-shift analyses. In those computational procedures η is sometimes either artificially smoothed to 1, unphysically greater than 1, or disconnected.⁴ The agreement of the predictions of this work with the (independent) work at Saclay is good. The elastic scattering data do not prefer one set of values of η_{lJ} over another, and so are not useful in determining the energy dependence of δ_{00} .

VII. P_{11} BRANCHING RATIO

Assuming that πN , $\pi\Delta$, and σN are the only open channels, total amplitudes for decay of the P_{11} intermediate state can be determined from these fits to the model. Since the inelastic processes are coherent, individual rates for the $\pi\Delta$ and σN decays cannot be inferred. The relative magnitudes of the various decay amplitudes provide a measure of the coupling of the P_{11} isobar to the $\pi\Delta$ and σN even though the interpretation

TABLE X. P_{11} branching ratios calculated from the fits to the data.

	πN	$\pi\Delta$	σN
"C" solutions			
(MeV)			
1340	0.43 ± 0.05	0.03 ± 0.05	0.54 ± 0.05
1370	0.60 ± 0.10	0.04 ± 0.12	0.36 ± 0.12
1400	0.63 ± 0.07	0.09 ± 0.10	0.28 ± 0.10
1400	0.67 ± 0.18	0.03 ± 0.20	0.30 ± 0.20
(both states fitted)			
"V" solutions			
1340	0.42 ± 0.17	0.22 ± 0.17	0.36 ± 0.17
1370	0.50 ± 0.16	0.23 ± 0.16	0.27 ± 0.16
1400	0.54 ± 0.10	0.23 ± 0.10	0.23 ± 0.10
1400	0.58 ± 0.09	0.22 ± 0.12	0.20 ± 0.12
(both states fitted)			

⁴⁶ M. de Beer, B. Deler, J. Dolbeau, M. Neveu, Nguyen Thuc Diem, G. Smadja, and G. Valladas Nucl. Phys. B12, 599 (1969).

⁴⁷ A. T. Davies, Glasgow report, 1969 (unpublished).

as decay branching ratios is tenuous at best. Further, even ignoring the interference term in the decay intensity, there is still uncertainty in the interpretation of the relative magnitudes of the $\pi\Delta$ and σN amplitudes, since the maximum c.m. energy in this work does not reach the resonance maximum. Also, no attempt has been made to separate resonance from possible background amplitudes.

Using the fitted $PP1$ and $PS1$ amplitudes, ignoring the interference between $\pi\Delta$ and σN , together with the CERN theoretical values of the πN elastic scattering phase shift δ_{11} , one obtains the branching ratios given in Table X. The "cross" terms in the square of the sum of amplitudes is approximately 20% of the diagonal terms for the V solutions, and consistent with zero for the C solutions. The relative couplings to $\pi\Delta$ and σN deduced from the fits depend strongly on the character of the object called σ . In the C solutions, the $\pi\Delta$ coupling is very small, whereas in the V solution the $\pi\Delta$ mode is comparable in strength with σN , becoming relatively more important as the energy increases.

VIII. SUMMARY OF CONCLUSIONS

The "Kirz anomaly,"¹ that is, the high-mass peak in the $\pi^+\pi^-$ spectrum in $\pi^-p \rightarrow \pi^+\pi^-n$, has been explained over a range of incident π^- momenta by the introduction of an $I=J=0$ $\pi\pi$ interaction. All the features of $\pi^-p \rightarrow \pi^-p\pi^0$ have been fitted without any $I=J=1$ $\pi\pi$ interaction. There is a discrepancy of marginal statistical significance between theory and experiment in the shape of the $\pi^-\pi^0$ (mass)² spectrum, the experimental spectrum being more sharply peaked. The data of the Saclay group⁴⁶ at 530 MeV/c show the same effect.

Two types of energy dependence of δ_{00} have been considered (Fig. 15). In the Veneziano-Lovelace⁴⁰ form, δ_{00} rises approximately linearly from threshold, passing through 90° near 720 MeV: The other form has δ_{00} rising from threshold as q^3 for energies less than 450 MeV and would give a narrower resonance than the first form. It has not been necessary to invoke a resonance with peak in the mass range investigated. The results favor the q^3 form since the χ^2 are consistently better.

However, some modifications retaining the basic Veneziano-type $\pi\pi$ interaction might give a better fit.

The Veneziano fit, including the $\pi\Delta$ mechanism, is far better than that of Roberts and Wagner⁴⁸ to fewer data.

There is substantial Δ production at incident momenta as low as 456 MeV/c (1339-MeV c.m.) rather far below the threshold for production of a Δ of mass 1236 MeV.

With the results of the fit to "isobar" model predictions, we have calculated partial-wave inelasticities in the S_{11} , P_{11} , P_{13} , D_{13} , and D_{33} partial waves, as a function of energy.

These results are only qualitatively in agreement with those following from the CERN elastic phase-shift analysis.⁸ We find inelasticity in the S_{11} , P_{13} , and D_{13}

⁴⁸ R. G. Roberts and F. Wagner, *Nuovo Cimento* **64A**, 206 (1969).

waves at lower energies than that analysis. The increasing inelasticities obtained here are consistent with the interpretation that P_{11} and D_{13} waves resonate at energies higher than those available in the present experiment.

The results of our analysis and that of the Saclay group⁴⁶ from 530 to 760 MeV/c are compatible.

We have derived values of the P_{11} branching ratios into πN , $\pi\Delta$, and σN where σ is an $I=J=0$ interacting $\pi\pi$ pair. The πN branching ratio is between 43% at 1339 MeV and 60% at 1402 MeV. The branching ratio between $\pi\Delta$ and σN depends, not surprisingly, on the form of σ used. In the preferred form the inelasticity is almost entirely through σN : With the Veneziano-Lovelace form of δ_{00} the ratio of $\pi\Delta$ to σN couplings is about unity and increases with energy.

Measurement of the K^- Cascade Time in Liquid Helium*

J. G. FETKOVICH, J. MCKENZIE,† B. R. RILEY, AND I-T. WANG

Carnegie-Mellon University, Pittsburgh, Pennsylvania 15213

AND

K. BUNNELL‡

Argonne National Laboratory, Argonne, Illinois 60439 and Northwestern University, Evanston, Illinois 60201

AND

M. DERRICK, T. FIELDS, L. G. HYMAN, AND G. KEYES§

Argonne National Laboratory, Argonne, Illinois 60439

(Received 21 May 1970)

The average cascade time of K^- mesons has been measured in a helium bubble chamber. In a sample of about 36 000 stopped K^- , 44 τ decays at rest were found, corresponding to a cascade time of $(3.2 \pm 0.5) \times 10^{-10}$ sec. This result agrees with a previous measurement.

INTRODUCTION

WHEN a negative meson stops in a material medium, it forms a mesonic atom with a constituent nucleus by replacing an electron. The meson, initially in a highly excited level, cascades down through the lower levels accessible to it until it decays or undergoes a nuclear reaction. It is sometimes important to know the atomic state from which nuclear capture occurs. For this reason, studies of the cascade process are necessary.

The first detailed attempt to understand the cascade process in liquid helium was made in a theoretical study by Day.¹ One might expect naively that in

helium both electrons are rapidly ejected by internal Auger transitions, and then the K -mesonic ion further deexcites by electromagnetic transitions. If so, the cascade would go through circular orbits, and nuclear interactions might be expected to proceed mainly from the $3d$ and $2p$ states. Day showed that collisional effects might be important enough to considerably modify that expectation. In particular, he concluded that because of collisional Stark-effect mixing of orbital angular momentum states, most π^- and K^- would undergo nuclear capture from relatively high s states.

It is possible also to study the cascade process experimentally. The easiest parameter to measure is the average cascade time. The two measurements^{2,3} of the

* Work performed under the auspices of the U. S. Atomic Energy Commission.

† Now at University College, London, England.

‡ Now at Stanford Linear Accelerator Center, Stanford, Calif. 94305.

§ Now at Université Libre de Bruxelles, Bruxelles, Belgium.

¹ T. B. Day, *Nuovo Cimento* **18**, 381 (1960).

² J. G. Fetkovich and E. G. Pewitt, *Phys. Rev. Letters* **11**, 290 (1963).

³ M. M. Block, T. Kikuchi, D. Koetke, J. B. Kopelman, C. R. Sun, R. Walker, G. Culligan, V. L. Telegdi, and R. Winston, *Phys. Rev. Letters* **11**, 301 (1963). The final result of the experiment is given in Ref. 4.